Nanoscale

Accepted Manuscript

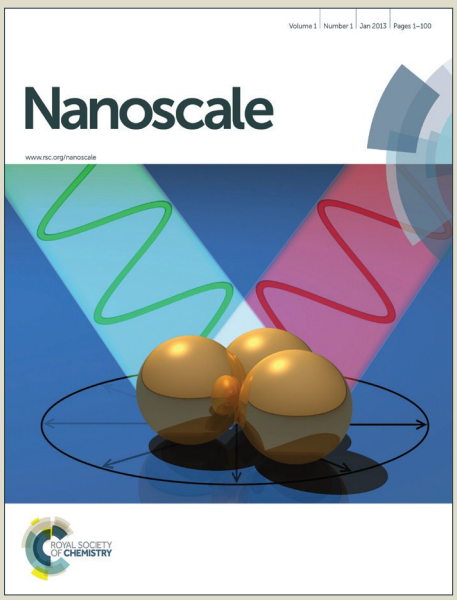

ROYAL SOCIETY OF CHEMISTRY

www.rsc.org/nanoscale

Journal Name

ARTICLE TYPE

Cite this: DOI: 10.1039/xxxxxxxxxx

Coherent transport through spin-crossover magnet Fe_2

Jing Huang,*[a,b] Rong Xie,[a] Weiyi Wang,[b] Qunxiang Li*[b,c] and Jinlong Yang[b,c]

Received Date
Accepted Date

DOI: 10.1039/xxxxxxxxxx

www.rsc.org/journalname

As one of the most possible building blocks in molecular spintronics, spin crossover (SCO) complexes have been attracted increasing attention due to their magnetic bistability between the high-spin (HS) and low-spin (LS) states. Here, we explore the electronic structures and transport properties of SCO magnets Fe_2 with three different spin-pair configurations, namely [LS-LS], [LS-HS], and [HS-HS], by performing extensive density functional theory calculations combined with non-equilibrium Green's function technique. Our calculations clearly reveal that the SCO magnet Fe_2 complexes should display two-step spin transitions triggering by external stimuli, i.e. temperature or light, which confirm the previous phenomenological model and agree well previous experimental measurements. Based on the calculated transport results, we observe nearly perfect spin-filtering effect and negative differential resistance (NDR) behavior integrating in SCO magnet Fe_2 junction with the [HS-HS] configuration. The current through the [HS-HS] SCO magnet Fe_2 under small bias voltage is mainly contributed by the spin-down electrons, which is significantly larger than that of the [LS-LS] and [LS-HS] cases. The bias-dependent transmissions are responsible for the observed NDR effect. These theoretical findings suggest that SCO Fe_2 complexes hold potential applications in molecular spintronic devices.

1 Introduction

In the past years, molecular spintronics, which combines the contemporary exploitation of the electron and spin degrees of freedom at single-molecule level,[1–4] has attracted considerable attention since it holds promise for the next generation of electronic devices with enhanced functionality and improved performance, especially in quantum computing and high-density information storage.[5–7]Based on magnetic molecules, i.e. organometallic wire, metal phthalocyanines, metal clusters, magnetic C_{28} molecule, and molecular magnets,[5,8–11] various spin devices including spin filtering, spin valves, and spin crossover (SCO), have been successfully demonstrated in experiments or have been theoretically proposed.[12,13]

As one of the most possible building blocks in molecular spintronics, SCO complexes have been attracted increasing attention due to their magnetic bistability.[14,15] In general, SCO complexes containing a transition metal ion that can be switched between a low-spin (LS) and a high-spin (HS) state by diverse external stimulus, such as temperature, light, pressures, magnetic or electric fields or charge flow, have wide applications in information storage and molecular sensor.[16–20] Previous investigations mainly focused on SCO complexes with a pseudo-octahedral molecular first-row transition metal ion, which has a d^4-d^7 electron configuration[21,22] Since the first discovered Fe dithiocarbamate complexes in 1931,[23] the mononuclear Fe family with the Fe coordinated to six N atoms (FeN_6) has been extensively investigated to display rather easy controlled spin-crossover electronic and transport properties.[24,25] The HS state in Fe(II) complexes (d^6)[26–29] is described by a $t_{2g}^4 e_g^2$ electron configurations, while the LS state has t_{2g}^6 configuration. Recently, special attention has been paid to binuclear SCO complexes, which occupy a special place among polynuclear spin transition systems.[30–32] Although the number of binuclear SCO complexes is very limited, their SCO behavior has been investigated by several experimental and theoretical groups.[33] Three different types of magnetic behaviors in binuclear SCO complexes, such as one step directly from [HS-HS] to [LS-LS] spin-pair electronic configuration, two-step from [HS-HS] to [LS-LS] via a plateau [LS-HS] configuration, and partial [HS-HS]↔[LS-HS] spin transitions, have been revealed.[34–36]

However, electron transport experiments in binuclear SCO

[a]School of Materials and Chemical Engineering, Anhui Jianzhu University, Hefei, Anhui 230601, China. E-mail: jhuang@ustc.edu.cn
[b]Hefei National Laboratory for Physical Sciences at the Microscale, University of Science and Technology of China, Hefei, Anhui 230026, China.E-mail: liqun@ustc.edu.cn
[c]Synergetic Innovation Center of Quantum Information and Quantum Physics, University of Science and Technology of China, Hefei, Anhui 230026, China

Electronic Supplementary Information (ESI) available: the spin density of SCO magnets Fe_2, the partial DOS of HS Fe cation, zero-bias transmission curves of SCO magnets Fe_2 junctions with different anchoring configurations, and bias-dependent transmission curves of SCO magnets Fe_2 with the [LS-LS] and [LS-HS] configurations. See DOI: 10.1039/x0xx00000x

complexes at the single molecular level remain scarce so far, mostly because depositing such complexes on surfaces with a controllable anchoring contact is very difficult.[37–39] Moreover, it is still an important challenge to explore the origin of different types of SCO in binuclear complexes since there is a simultaneous electronic and structural change of the molecule between two different spin-state isomers. In this work, the electronic structures and transport properties of SCO magnet Fe_2, namely, $Fe(dpia)(NCS)_2]_2(bpac)$, dpia=bis(2-picolyl)amine, bpac=1,2-bis(4-pyridyl)ethyne],[36] with the [LS-LS], [LS-HS] and [HS-HS] spin-pair configurations, are explored by performing extensive spin-polarized density functional theory (DFT) calculations combined with non-equilibrium Green's function method. We clearly reveal that SCO magnet Fe_2 complexes should display two-step spin transitions, which agrees with previous experimental measurements and theoretical predictions. Moreover, we find that nearly perfect spin-filtering effect and negative differential resistance (NDR) behavior coexist in SCO magnet Fe_2 junction with the [HS-HS] configuration, whose conductivity is mainly determined by the spin-down electrons under small bias voltages.

2 Computational model and methods

Electronic structures and coherent transport properties of SCO magnet Fe_2 are explored by performing DFT calculations combined with the non-equilibrium Green's functional method, implemented in ATK package,[40,41] which has been successfully used to explain many experimental results.[42,43] In our calculations, the generalized gradient approximation in the Perdew-Burke-Ernzerhof form is used to describe the exchange and correlation energy. The interaction between ionic cores and valence electrons is modeled with Troullier-Martins nonlocal pseudopotential. Double-zeta plus polarized basis sets are employed for all atoms. An energy cutoff is set to be 150 Ry for the real-space grid on which the Poisson equation is self-consistently solved. The spin-resolved transmission coefficients of these molecular junctions are obtained by

$$T_\sigma(E,V) = Tr[\Gamma_L G_\sigma \Gamma_R G_\sigma^+], \quad (1)$$

where σ stands for the spin-up ($\uparrow$) and spin-down ($\downarrow$) channels. G_σ is the spin-dependent retarded Green's function of the extended molecule, $\Gamma_{L/R}$ is the coupling matrix between the extended molecule and the left/right electrode. The current through the molecular junction is obtained by

$$I(V) = \frac{e}{h}\int T_\sigma(E,V)[f(E-\mu_L) - f(E-\mu_R)]dE, \quad (2)$$

here, the f(E-$\mu_{L(R)}$) is the Fermi-Dirac function for the left and right electrodes with the chemical potential $\mu_{L(R)}$. Based on the Landauer-Büttiker formula, the spin-up and spin-down electrons are coherent, indicating that the length of the active channel is less than the phase-breaking mean free path.

3 Results and discussion

We start with the geometric, electronic and magnetic properties for the isolated SCO magnet Fe_2 with three different spin-pair configurations, which are rather difficult since the relative e[illegible] difference between two isomers is sensitive not only to the choic[illegible] of exchange and correlation functionals but also to the atomi[illegible] laxation.[44] In our calculations, the initial structures for the LS-[illegible] and HS-HS states is taken from the low-, and high-temper[illegible]e structures in experiments,[36] respectively. And we suppose th[illegible] the isolated SCO magnet Fe_2 structures with [LS-LS] and [HS-HS] spin-pair configurations possess a center of symmetry [illegible] moiety of the departure structure of SCO magnet Fe_2 wit[illegible] the [LS-HS] configuration is taken from one half of the [LS-LS] [illegible] while another moiety from half of the [HS-HS] case, and t[illegible] fully relax all atomic positions to obtain the correspondi[illegible] timized structure. The calculated total energy results show [illegible] the order of total energies of SCO magnet Fe_2 is [LS-LS] [illegible] HS] < [HS-HS] configuration. Namely, the [LS-LS] case has the lowest energy, and the energy difference between [LS-[illegible] [HS-HS] configurations is predicted to be about 0.61 eV. I[illegible] tw[illegible] $[FeN_6]$ coordination cores of SCO magnet Fe_2 with the [LS-LS] and [HS-HS] configurations, the Fe-N distances are differen[illegible] fall within the range of [1.97, 2.09] and [2.04, 2.36] Å, r[illegible]spec[illegible] tively, as shown Fig. 1. The average Fe-N distance is 2.23 Å in the [HS-HS] configuration, which is longer about 0.20 Å than t[illegible] at [illegible] the [LS-LS] case. The NCS groups in these complexes have nearly linear geometry, and the Fe-Fe separation through the spac[illegible] is and in the [HS-HS] and [LS-LS] spin-pair configurations is 14.25 and 13.79 Å, respectively. The relative longer Fe-N distan[illegible]es i[illegible] pseudo-octahedral coordination lead to the local relatively weak FeN_6 crystal field, corresponding to the [HS-HS] configur[illegible]tio[illegible] The $3d^6$ electrons of Fe(II) cores in SCO magnet Fe_2 with [LS-LS] the and [HS-HS] spin-pair configurations can be describe[illegible]d by t[illegible]wo $t_{2g}^6 e_g^0$ and $t_{2g}^4 e_g^2$ electron configurations, and correspond to two sin[illegible]glet (S=0) and quintet (S=2) spin-states, respectively. The magnetic moments of SCO magnet Fe_2 with the [LS-LS], [LS-HS] a[illegible] [HS-HS] configurations are predicted to be 0.0, 4.0 and 8.0 μ_B (Bohr magneton). The spin density distribution illustrates that the magnetism is mainly contributed by the HS Fe cations (Fig. S1). These optimized Fe-N distances and predicted magnetic moments agree well with previous experimental results.[36]

Moreover, we find that the spatial distribution and the energy positions of the frontier orbitals are dramatically different fo[illegible] w[illegible] different spin-pair configurations. The bottom panel of Fig. 1 (a) and (b) presents the spatial profiles of the highest occupie[illegible] molecular orbital (HOMO) and the lowest unoccupied molecular orbital (LUMO) of SCO magnet Fe_2 with the [LS-LS] and [HS-HS] configurations, respectively. As for SCO magnet Fe_2 with the [LS-LS] configuration, the ground state of this isolated co[illegible]ple[illegible] is nonmagnetic. The HOMO localizes around the ligands, while the LUMO delocalize over the entire complex, which lies at -4.[illegible]07 and -3.57 eV, respectively. It is clear that for the [HS-HS] [illegible]g[illegible] uration, as shown in Fig. 1(b), SCO magnet Fe_2 is spin-polarized and two spin channels display different features. The energy gap for the spin-up electrons is about 1.39 eV, which is remarkably

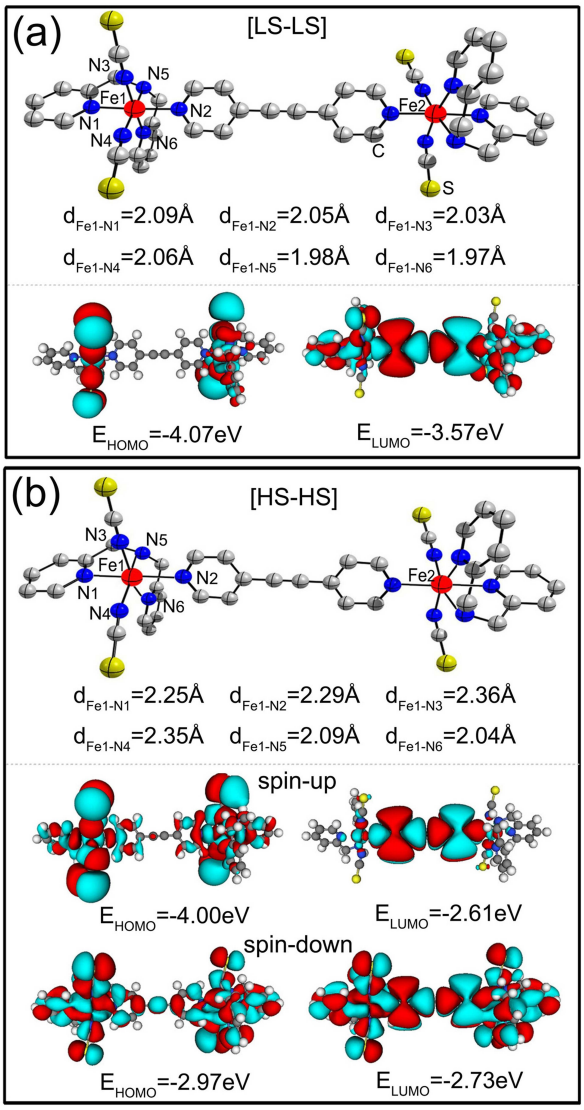

Fig. 1 (Color online) The optimized structures and spatial distribution of the HOMO and LUMO of SCO magnet Fe_2, (a) for the [LS-LS], and (b) for the [HS-HS] spin-pair configuration.

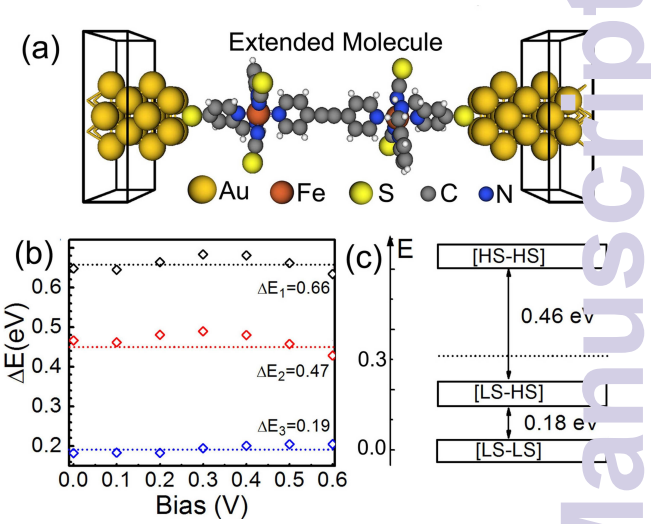

Fig. 2 (a) Schematic illustration of the proposed junction, here, SCO magnet Fe_2 is sandwiched between two Au(100) electrodes. (b) Change of the relative total energies (in eV) under bias voltages. The black, red and blue symbol-lines stand for the averaged total energy differe between [HS-HS] and [LS-LS], [HS-HS] and [LS-HS], and [LS-HS] and [LS-LS] configurations, labeled with ΔE_1, ΔE_2 and ΔE_3, respectively. (c) Relative energies of the [LS-LS], [LS-HS] and [HS-HS] spin-pair configurations, and the dashed lines indicate the average energy (0.[illegible] eV) between the [LS-LS] and [HS-HS] configurations.

larger than the gap of the spin-down electrons (0.24 eV). The HOMO and LUMO of the spin-down electrons locating at -2.97 and -2.73 eV are delocalized over the entire complex, while the spin-up HOMO localizes around the ligands and the LUMO localizes around the central region, which locates at -4.00 and -2.61 eV, respectively. These observed remarkably differences in the geometric and electronic structures of SCO magnet Fe_2 with different spin-pair configurations suggest that they are possible candidates for designing molecular spintronic devices with interesting transport behavior.

Before investigating the transport properties of SCO magnet Fe_2 junctions, as shown in Fig. 2(a), we turn to explore the effective method to realize the spin transition from the [LS-LS] to [HS-HS] configuration in SCO magnet Fe_2, since many experimental and theoretical investigations have revealed that various external stimuli, such as temperature, light, pressure, magnetic or electric fields, SCO complexes can be switched between two different spin-pair cases.[14] Firstly, we calculate the influen[illegible] of an electric field (arising from the applied bias voltage be[illegible] the left and right electrodes) on the relative total energies [illegible] molecular junctions with three different spin-pair configura[illegible]. Here, ΔE_1, ΔE_2, and ΔE_3 is defined as the averaged total e[illegible] difference between [HS-HS] and [LS-LS], [HS-HS] and [LS-HS], and [LS-HS] and [LS-LS] configurations, respectively. We f[illegible] the influence of an electric field on the relative total ene[illegible] ifferences to be relatively small. As shown in Fig. 2(b), in the bias voltage range of [0, 0.6] V, ΔE_1, ΔE_2, and ΔE_3 is predicted to be about 0.66, 0.47, and 0.19 eV, respectively, and all of them var[illegible] within 0.05 eV. For example, a bias voltage of 0.6 V just modifies ΔE_1, ΔE_2, and ΔE_3 only about 0.026, 0.042, 0.015 eV, respectively. These observations imply that an electric field in these exa[illegible] molecular junctions can not directly induce the spin transition in SCO magnet Fe_2 complexes, although for electronic applic[illegible] it is more preferable to achieve a spin crossover transition purely by electric field.[18] Note that spin crossover transition by [illegible] of an electric field can be achieved for Fe-based single-mole[illegible] magnets and Co-based valence tautomeric compounds.[21,2[illegible]]

From these calculated total energies for the SCO magnet Fe[illegible] molecular junctions, we find that the mixed [LS-HS] one falls in the energy gap between the [LS-LS] and [HS-HS] configurations, as shown in Fig. 2(c). According to the phenomenol[illegible] model,[34] its position relative plays an important role in the shaping of the spin transition. To have a two-step spin transition, [illegible] relative energy of SCO magnet Fe_2 with [LS-HS] confi[illegible] must be lower than the halfway point of the energy gap between the [LS-LS] and [HS-HS] configurations. The averaged total energies between the [LS-LS] and [HS-HS] configurations is predicted

to be about 0.32 eV, which is slightly larger than that of the relative energy (0.18 eV) of the [LS-HS] case. This observation agrees well with the experimental observation,[36] which means that the SCO magnet Fe_2 complexes should display two-step transitions. Clearly, as for the SCO magnet Fe_2, our calculated results confirm the phenomenological model.[34]

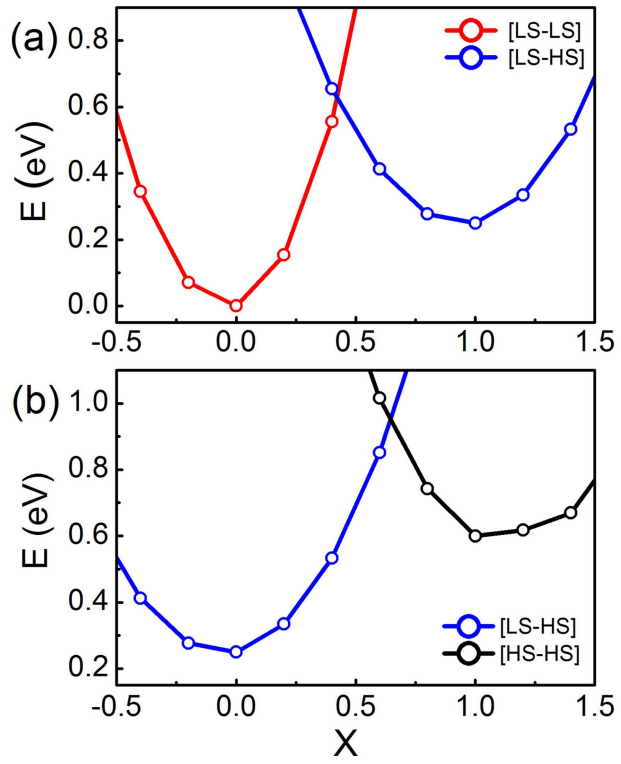

Fig. 3 (a) At the GGA level, the relative total energies (in eV) of the isolated SCO magnet Fe_2 complexes with the [LS-LS] and [LS-HS] configurations along the reaction coordinates, X. (b) The relative total energies (in eV) for the [LS-HS] and [HS-HS] configurations along X.

To estimate the energy barriers of the two-step spin transitions of SCO magnet Fe_2 complexes, we calculate the total energies of these isolated SCO magnet Fe_2 complexes as a function of the reaction coordinates (X), and plot them in Fig. 3(a) and (b). As for the spin transition between the [LS-LS] and [LS-HS] configurations, as shown in Fig. 3(a), X is interpolated between the [LS-LS] (X=0) and the [LS-HS] (X=1) geometry for the two different spin-pair configurations. Here, the reaction coordinate projected out of the Hessian matrix is defined as the difference in the local Fe-N distances via normal mode analysis. As expected, Fig. 3(a) clearly shows that the ground state of SCO magnet Fe_2 is low spin, corresponding to the [LS-LS] spin-pair configuration. As X increases, originating from the weakening of the local FeN_6 ligand field, there is a transition from the [LS-LS] to [LS-HS] for X∼0.42, and the transition barrier is predicted to be about 0.61 eV. While for the spin transition between the [LS-HS] and [HS-HS] configurations, the transition barrier is about 0.93 eV at X∼0.7, as shown in Fig. 3(b). Two transition barriers have relative large values, implying that the two-step transitions, from the [LS-LS] to [HS-HS] via a plateau [LS-HS] configuration, can be triggered by external stimuli, i.e. temperature or light. Such transitions are accompanied with the geometrical structure modifications, which, at the same time, alter the local FeN_6 crystal field strength.[36] That is to say, the two-step spin transitions of the Fe_2 complexes can be realized by changing the metal-to-ligand bond distances via external stimuli. Then the weak and strong FeN_6 crystal fields correspond to the Fe(II) magnetic bistability of SCO Fe_2 complex with the [HS-HS] and [LS-LS] spin-pair configurations, respectively.

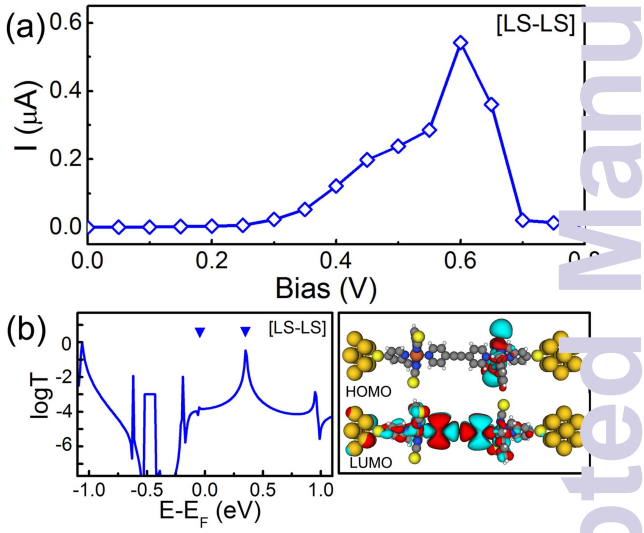

Fig. 4 (a) The calculated I-V curve of SCO magnet Fe_2 with the [LS-LS] configuration. (b) The spin-resolved zero-bias transmission function and the spatial distribution of the LDOS at the perburbed HOMO and LUMO, which is labelled with two upside-down triangles.

Since the exact anchoring configuration of molecular devices in experiments is a 'blackbox' so far, here, we propose several SCO magnet Fe_2 complex junctions with different anchoring configurations to explore their transport properties. For example, to model the molecular junction with one more different anchoring groups, the SCO magnet Fe_2 complex with the [HS-HS] and [LS-LS] configurations are sandwiched between two Au(10) nanoelectrodes via both thiol and thiocyanato end groups. Fig. S2 shows the proposed molecular junction and the corresponding zero-bias transmission curves. To model the same electrode material with different crystal surface and to simulate the SCO magnet Fe_2 monolayer case, Fig. S3 and S4 present the calculated results of one SCO magnet Fe_2 complex sandwiched between two periodic Au(111) electrodes using 6×6 supercells and two SCO magnet Fe2 complexes connected to two periodic Au(100) electrodes using 8×8 supercells, respectively. Note that such a anchoring configuration of the SCO magnet Fe_2 complexes sandwiched between two Au electrodes via thiol groups is commonly adopted in molecular electronics, although the nature of the Au-S bond and the reacting species involved in the connections need carefully check.[45]

Here, as examples, SCO magnet Fe_2 with different spin-pair configurations are sandwiched between two Au(100) nanoelectrodes. Through calculating the adsorption energies, we find that SCO magnet Fe_2 prefers to adsorb on the hollow sites of Au(100) surface via Au-S bonds, as shown in Fig. 2(a). The proposed two-

probe systems can be divided into three parts, including the left and right electrodes, and the central extended molecule containing the sandwiched SCO magnet Fe_2 and two and three surface layers of the left and right electrodes, respectively, where all the screening effects are included into the contact region, and charge distribution in the electrodes is the same as that of the bulk phase. Here, the Au-S distance is fixed to be about 2.59 Å, which is close to the adopted value in the previous investigations.[46] Note that the geometric and electronic structures of SCO magnet Fe_2 are slightly disturbed by the Au(100) electrodes. The magnetic moment of SCO magnet Fe_2 junction with the [HS-HS] configuration is predicted to be about 8.4 μ_B. The calculated partial density of states of Fe 3d orbitals, as shown in Fig. S5, imply that the HS Fe cation still has the $t_{2g}^4 e_g^2$-like electron configuration.

Firstly, we examine the energetically preferring structure of SCO magnet Fe_2, namely, the complex has the [LS-LS] configuration, which corresponds to the low-temperature structure observed in experiments.[36] The SCO magnet Fe_2 junction is nonmagnetic since both local strong FeN_6 crystal fields ensure spin-pair states (two singlets, S=0). The calculate spin-restricted I-V curve is shown Fig. 4(a). Here, at each bias voltage, the current is determined self-consistently under the non-equilibrium condition. It is clear that the I-V curve displays nonlinear feature and an obvious NDR effect. With increasing of bias voltage, the maximum current is about 0.54 μA at the peak position (V_{bias} =0.6 V), while the current reaches its minimum value (0.005 μA) at the valley site (V_{bias} = 0.8 V), which leads to a large peak-valley rate (PVR) of about 100. To explore the nature of transport behavior of SCO magnet Fe_2 with the [LS-LS] configuration, the zero-bias transmission function and the local density of states (LDOS) are plotted in Fig. 4(b). Here, two upside-down triangles stand for the perturbed HOMO and LUMO due to the presence of the Au(100) electrodes. Clearly, comparing with the spatial distribution of the HOMO and LUMO of the isolated SCO magnet Fe_2 complexes, as shown in Fig.1, the significant transmission peak at 0.35 eV is mainly contributed by the perturbed LUMO, which is delocalized over the whole complex. Due to the localization, the perturbed HOMO does not lead to a transmission peak at all. The energy separation between the perturbed HOMO and LUMO is about 0.4 eV, which is slightly less than that of the energy space (0.5 eV) between the HOMO and LUMO of the isolated SCO magnet Fe_2 with the [LS-LS] configuration. As for the mechanism of NDR behavior, we will address later.

As we discussed above, SCO magnet Fe_2 with the mixed [LS-HS] configuration is the intermediate structure for the two-step spin transitions, as shown in Fig. 5(a), which mixes the geometric and electronic structures of the [LS-LS] and [HS-HS] spin-pair configurations. In this case, one of two Fe(II) has the S=2 spin state, while the other Fe(II) has the S=0 spin state. That is to say, SCO magnet Fe_2 with the [LS-HS] configuration is spin-polarized. The spin-resolved I-V curves and the zero-bias transmission spectra are calculated and presented in Fig. 5(b) and (c), respectively. Under small bias voltage, the conductance of SCO magnet Fe_2 with the [LS-HS] configuration mainly transport through the spin-down electrons. The transmission coefficients of the spin-down electrons around the Fermi level are larger than that of the

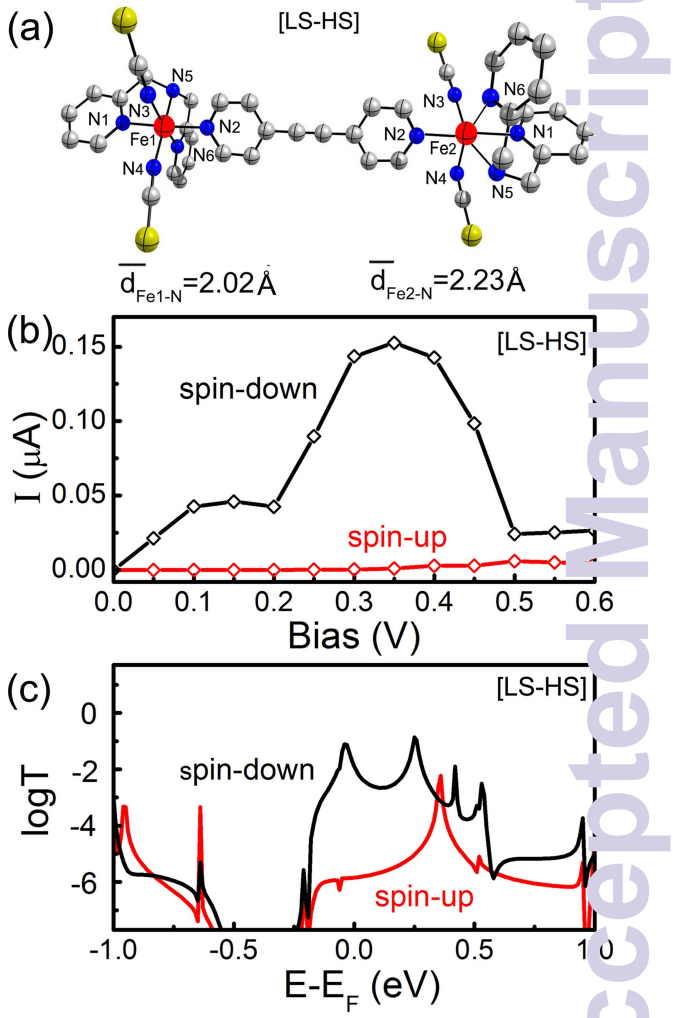

Fig. 5 (a) The optimized geometric structure of SCO magnet Fe_2 with the [LS-HS] configuration, (b) The spin-resolved I-V curves. (c) The zero-bias transmission functions and the spatial distribution of the LDOS at the perburbed HOMO and LUMO for the spin-up and spin-down electrons.

spin-up electrons, which results in an obvious spin-filtering effect within a certain bias range, i.e. [-0.1, 0.4] V. Moreover, the NDR behavior appears again. The maximum and minimum $I_\downarrow$ is about 0.16 and 0.02 μA, which locates at 0.35 and 0.5 V, respectively. Note that the current through SCO magnet Fe_2 with the [LS-HS] configuration is slightly less than that of the [LS-LS] case.

Finally, we turn to explore the transport properties of SCO magnet Fe_2 with the [HS-HS] configuration, in which two Fe atoms locate in the weak FeN_6 crystal fields due to the long Fe-N separations. The high-spin state of two Fe(II) in this case is characterized by S=2. This results in the magnetic moment of SCO magnet Fe_2 with the [HS-HS] configuration is about 8 μB. Fig. 6(a) shows the spin-resolved I-V curves. Here, the the red and black lines stand for the current through the spin-up and spin-down electrons, respectively. The following features are observed.

(i) The current through SCO magnet Fe_2 with the [HS-HS] configuration is significantly larger than that of the [LS-LS] and [LS-HS] cases. For example, at the bias voltage of 0.25 V, the current

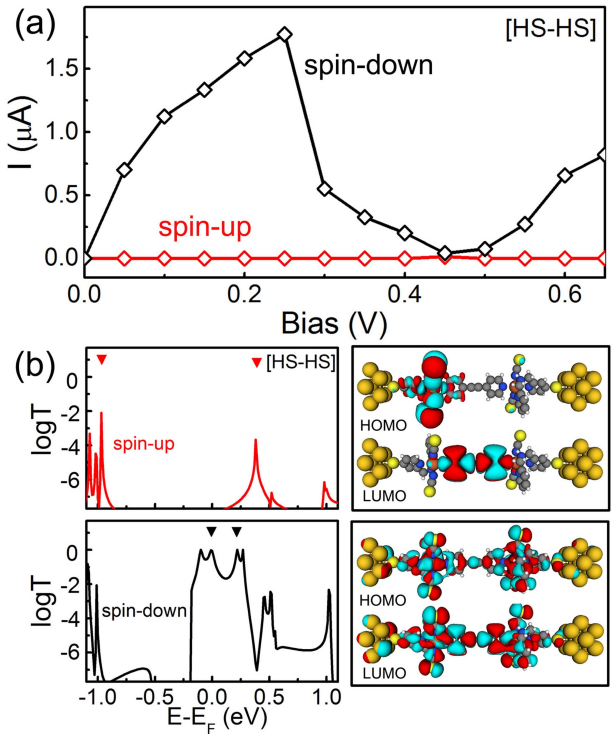

Fig. 6 (a) The spin-resolved I-V curves through SCO magnet Fe_2 with the [HS-HS] configuration. (b) The spin-resolved zero-bias transmission functions for two spin channels and the spatial distribution of the perturbed HOMO and LUMO. Here, the red and black lines stand for spin-up and spin-down electron, respectively.

through SCO magnet Fe_2 with the [HS-HS], [LS-HS], and [LS-LS] spin-pair configurations is predicted to be about 1.77, 0.09, and 0.006 μA, respectively. That is to say, the former is larger about two orders than the later two cases.

(ii) As shown in Fig. 6(a), the obvious spin-filtering effect is observed for SCO magnet Fe_2 with the [HS-HS] configuration. At the bias voltage of 0.4 V, the calculated current is predicted to be about 3×10^{-5} and 0.20 μA for the spin-up and spin-down electrons, respectively. The current difference between two spin channels under different bias voltage can be quantified by the ratio of current defined as $R(V)=I_{\downarrow}/I_{\uparrow}$. The calculated R varies from 6500 to 32000 in the bias range of [0.1, 0.4] V. This conductivity dominated by the spin-down electrons has been observed in many magnetic molecules, i.e. ironcyclooctatetraene (Fe−COT) clusters and iron phthalocyanine (FePc).[47,48]

(iii) At the same time, NDR phenomena is observed for SCO magnet Fe_2 junction with the [HS-HS] configuration. When the bias voltage is swept forward to 0.7 V from zero, the $I_{\downarrow}$ initially increases linearly to about 1.77 μA at 0.25 V. Then, upon approaching to 0.45 V, the $I_{\downarrow}$ drops to 0.04 μA. This results in a significant NDR behavior with a peak-to-valley ratio of about 25, which is readily measurable in experiments.

(iv) Clearly, a dual functionality, nearly perfect spin-filtering effect and obvious NDR, is integrated in SCO magnet Fe_2 junction with the [HS-HS] configuration. Of course, this remarkably coexisting of spin-filtering effect and NDR in SCO magnet Fe_2 junction highlights its promising potential for molecular electronic applications, i.e. fast switch devices and logic gates.

To understand the nature of the observed spin filter effect in SCO magnet Fe_2 with the [HS-HS] configuration, it is useful to look into the spin-polarized zero-bias transmission curves and the spatial distributions of the perturbed HOMO and LUMO, as shown in Fig. 6(b), in which, the filled upside-down triangles stand for molecular projected self-consistent Hamitonian states. It is clear that the transmission spectra of SCO magnet Fe_2 for two spin channels display remarkably different behaviors around the Fermi level. The transmission coefficients of the spin-up channel are quite small in the energy region from -0.80 to 0.1 eV. Two sharp and low transmission peaks locates are -0.95 and 0.35 eV, which is contributed by the localized HOMO and LUMO, respectively, as shown in the right panel of Fig. 6(b). While for the spin-down electrons, the delocalized HOMO and LUMO provide the near perfect conductance channels through the molecular junction, which lead to the transmission coefficients at -0.10 and 0.27 eV close to 1 G_0 (G_0 denotes the quantum constant and equals to e^2/h). The distinct difference of transmission spectrum between two spin channels can be evaluated with spin filter efficiency, SFE, defined as $(T_{\uparrow}-T_{\downarrow})/(T_{\uparrow}+T_{\downarrow})$, at the Fermi level. Here, $T_{\uparrow}$ and $T_{\downarrow}$ stands for the transmission coefficient of the spin-up and spin-down electrons, predicted to be 1×10^{-5} and 0.9 at the Fermi level, respectively. The calculated SFE at zero bias is 99.9 %, which indicates that conductance through SCO magnet Fe_2 with the [HS-HS] configuration is mainly governed by the spin-down electrons.

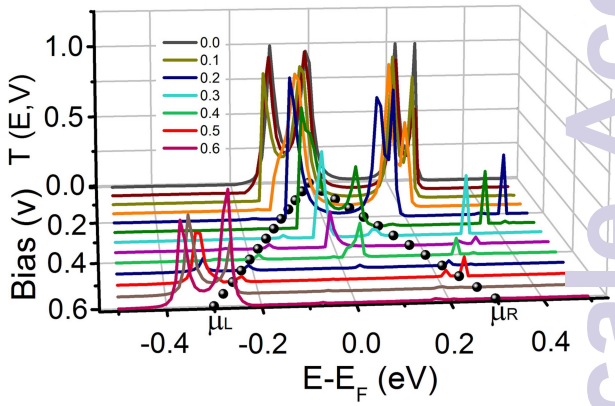

Fig. 7 The bias-dependent transmission functions for the spin-down electrons in SCO magnet Fe_2 with the [HS-HS] configuration. The dash-dotted short-dotted line points out the positions of the left and right chemical potentials(μ_L and μ_R).

To elucidate the NDR mechanism for SCO magnet Fe_2 with the [HS-HS] configuration, we calculate the bias-dependent transmission spectra since their shape and position will change under the applied bias voltage. Fig. 7 shows the transmission spectra under the bias voltage range [0.0, 0.6] V for the spin-down electrons. It is clear that the values of transmission coefficient change dramatically under the applied bias. With gradually increasing of the applied bias voltage, two transmission peaks around the Fermi level contributed by the HOMO and LUMO, which gives the dom-

inant contribution to the current through SCO magnet Fe_2, fuse into a transmission peak at 0.15 V. Then it gradually becomes narrow and small, and disappears at about 0.45 V. The current through the sandwiched complex is determined by the integral area under the transmission curve with the bias window. When the bias voltage is less than 0.25 V, there is a relative large integral area due to the transmission peaks around the Fermi level contributed by the HOMO and LUMO. The current increases with increasing of the bias voltage. When the applied voltage continuously increases, the fused transmission peak becomes narrow and small, and results in the reduction of the current. So the NDR behavior is observed. The $I_{\downarrow}$ initially increases, and reaches its maximum (1.77 μA) at 0.25 V, Then it decreases and reaches its minimum (0.043 μA) at 0.45 V. Such a bias-dependent transmission induced NDR behavior has been observed in other molecules, i.e. phenalenyl and four-coordinate Fe complex.[49,50]

4 Conclusions

In summary, based on DFT calculations combined with non-equilibrium Green's function technique, we explore the electronic and transport properties of SCO magnet Fe_2 complexes with the [LS-LS], [LS-HS] and [HS-HS] spin-pair configurations. We clearly reveal that two-step spin transitions in SCO magnet Fe_2 can be achieved by external stimuli, i.e. temperature or light, which agrees well with previous experimental observations and confirm the previous phenomenological model. The SCO magnets Fe_2 junction with the [HS-HS] configuration has high spin-filtering efficiency and obvious NDR phenomenon. Under a small bias voltage, the current through the [HS-HS] SCO magnets Fe_2 is mainly contributed by the spin-down electrons, which results in nearly perfect spin-filtering effect. The observed NDR phenomenon originates from the bias-dependent transmissions. Theoretical findings suggest that SCO Fe_2 complexes hold the great promising applications in molecular electronic devices.

Acknowledgements

This work was partially supported by National Key Basic Research Program (Nos. 2011CB921400 and 2014CB921101), by the Strategic Priority Research Program (B) of the CAS (No. XDB01020000), by the National Natural Science Foundation of China (Nos. 21273208 and 21473168), by Anhui Provincial Natural Science Foundation (Nos. 1408085QB26), and by the Innovative Program of Development Foundation of Hefei Center for Physical Science and Technology. Computational resources have been provided by CAS, Shanghai and USTC Supercomputer Centers.

References

1 S. A. Wolf, D. D. Awschalom, R. A. Buhrman, J. M. Daughton, S. von Molnár, M. L. Roukes, A. Y. Chtchelkanova and D. M. Treger, *Science*, 2000, **294**, 1488.

2 A. R. Rocha, V. M. García-Suárez, S. Bailey, C. J. Lambert, J. Ferrer and S. Sanvito, *Nat. Mater.*, 2005, **4**, 335.

3 S. Sanvito, *Chem. Soc. Rev.*, 2011, **40**, 3336.

4 S. D. Jiang, K. Goβ, C. Cervetti and L. Bogani, *Sci. China Chem.*, 2012, **55**, 867.

5 B. Lapo and W. Wolfgang, *Nat. Mater.*, 2008, **7**, 179.

6 J. Lehmann, A. Gaita-Ariño, E. Coronado and D. Loss, *J. Mater. Chem.*, 2009, **19**, 1672.

7 J. M. Clemente-Juan, E. Coronado and A. G.-A. no, *Chem. Soc. Rev.*, 2012, **41**, 7464.

8 Z. L. Yi, X. Shen, L. L. Sun, Z. Y. Shen, S. M. Hou and S. Sanvito, *ACS Nano*, 2010, **4**, 2274.

9 A. Candini, S. Klyatskaya, M. Ruben, W. Wernsdorfe n M. affronte, *Nano Lett.*, 2011, **11**, 2634.

10 S. M. Avdoshenko, I. N. Ioffe, G. Cuniberti, L. Dunsch an A. A. popov, *ACS Nano*, 2011, **5**, 9939.

11 Y. H. Zhou, J. Zeng, L. M. Tang, K. Q. Chen and H. P. Wu, *Org. Elect.*, 2013, **14**, 2940.

12 M. G. Zeng, L. Shen, Y. Q. Cai, Z. D. Sha and Y. P. Feng, *Appl. Phys. Lett.*, 2010, **96**, 042104.

13 R. R. Nair, I.-L. Tsai, M. Sepioni, O. Lehtinen, J. Keinonen, A. V. Krasheninnikov, A. H. C. Neto, M. I. Katsnelson, A. K. Geim and I. V. Grigorieva, *Nat. Commun.*, 2013, **4**, 2010.

14 A. Bousseksou, G. Molnár, L. Salmon and W. Nicolazzi, *Chem. Soc. Rev.*, 2011, **40**, 3313.

15 T. Miyamachi, M. Gruber, V. Davesne, M. Bowen, S. Boukari, L. Joly, F. Scheurer, G. Rogez, T. K. Yamada, P. Ohresser, E. Beaurepaire and W. Wulfhekel, *Nat. Commun.*, 2012, **3**, 938.

16 P. Gütlich, V. Ksenofontov and A. B. Gaspar, *Coord. Chem. Rev.*, 2005, **249**, 1811.

17 S. Ohkoshi, K. Imoto, Y. Tsunobuchi, S. Takano and H. Tokoro, *Nat. Chem.*, 2011, **3**, 564.

18 H. Hao, X. H. Zheng, L. L. Song, R. N. Wang and Z. Zeng, *Phys. Rev. Lett.*, 2012, **108**, 017202.

19 B. Warner, J. C. Oberg, T. G. Gill, F. E. Hallak, C. F. Hirjibehedin, M. Serri, S. Heutz, M. Arrio, P. Sainctavit, M. Mannini, G. Poneti, R.Sessoli and P. Rosa, *J. Phys. Chem. Lett.*, 2013, **4**, 1546.

20 R. Bertoni, M. Cammarata, M. Lorenc, S. F. Matar, J. F. Létard, H. T. Lemke and E. Collet, *Acc. Chem. Res.*, 2015, **48**, 774.

21 S. Hayami, Y. Komatsu, T. Shimizu, H. Kamihata and Y. H. Lee, *Coordin. Chem. Rev.*, 2011, **255**, 1981.

22 E. Cremades, C. D. Pemmaraju, S. Sanvito and E. Ruiz, *Nanoscale*, 2013, **5**, 4751.

23 L. Cambi and L. Szegö, *Ber. Dtsch. Chem. Ges.*, 1931, **64**, 2591.

24 P. Gütlich, Y. Garcia and H. A. Goodwin, *Chem. Soc. Rev.*, 2000, **29**, 419.

25 M. Nihei, T. Shiga, Y. Maeda and H. Oshio, *Coord. Chem. Rev.*, 2007, **251**, 2606.

26 D. Aravena and E. Ruiz, *J. Am. Chem. Soc.*, 2012, **134**, 777.

27 E. Ruiz, *Phys. Chem. Chem. Phys.*, 2014, **16**, 14.

28 H. Phan, S. M. Benjamin, E. Steven, J. S. Brooks and M. Shatruk, *Angew. Chem. Int. Ed.*, 2015, **127**, 837.

29 W. K. Zhang and K. J. Gaffney, *Acc. Chem. Res.*, 2015, **48**, 1140.

30 A. B. Gaspar, M. C. M. noz and J. A. Real, *J. Mater. Chem.*, 2006, **16**, 2522.

31 J. J. M. Amoore, S. M. . Neville, B. Moubaraki, S. S. Iremonger, K. S. Murray, J. Létard and C. J. Kepert, *Chem. Eur. J.*, 2010, **16**, 1973.

32 R. Kulmaczewski, J. Olguín, J. A. Kitchen, H. L. C. Feltham, G. N. L. Jameson, J. L. Tallon and S. Brooker, *J. Am. Chem. Soc.*, 2014, **136**, 878.

33 P. Maldonado, S. Kanungo, T. S. Dasgupta and P. M. Oppeneer, *Phys. Rev. B*, 2013, **88**, 020408(R).

34 S. Zein and S. A. Borshch, *J. Am. Chem. Soc.*, 2005, **127**, 16197.

35 G. S. Matouzenko, E. Jeanneau, A. Y. Verat and A. Bousseksou, *Dalton Trans.*, 2011, **40**, 9608.

36 G. S. Matouzenko, E. Jeanneau, A. Y. Verat and Y. Gaetano, *Eur. J. Inorg. Chem.*, 2012, **6**, 969.

37 A. Pronschinske, R. C. Bruce, G. Lewis, Y. F. Chen, A. Calzolari, M. Buongiorno-Nardelli, D. A. Shultz, W. You and D. B. Dougherty, *Chem. Commun.*, 2013, **49**, 10446.

38 G. Poneti, L. Poggini, M. Mannini, B. Cortigiani, L. Sorace, E. Otero, P. Sainctavit, A. Magnani, R. Sessoli and A. Dei, *Chem. Sci.*, 2015, **6**, 2268.

39 E. J. Devid, P. N. Martinho, M. V. Kamalakar, I. Šalitroš, Ú. Prendergast, J. Dayen, V. Meded, T. Lemma, R. González-Prieto, F. Evers, T. E. Keyes, M. Ruben, B. Doudin and S. J. van der Molen, *ACS Nano*, 2015, **4**, 4496.

40 J. Taylor, H. Guo and J. Wang, *Phys. Rev. B*, 2001, **63**, 245407.

41 M. Brandbyge, J.-L. Mozos, P. Ordejón, J. Taylor and K. Stokbro, *Phys. Rev. B*, 2002, **65**, 165401.

42 J. Huang, W. Y. Wang, S. F. Yang, Q. X. Li and J. L. Yang, *Nanotechnology*, 2012, **23**, 255202.

43 J. Huang, W. Y. Wang, Q. X. Li and J. L. Yang, *J. Chem. Phys*, 2014, **140**, 164703.

44 *Using Gaussian09 package, we obtain the optimized geometric structures of free SCO magnet Fe_2 isomers by using the Becke three-parameter Lee-Yang-Parr (B3LYP) hybrid functional, which this potential ensures a correct order of different spin states for experimental structures of mononuclear spin transition complexes at low and high temperatures. We find that the molecular magnetic moment and the spatial distribution of frontier molecular orbitals are not sensitive to the used functionals, and the hybrid DFT calculations enhance the level spacing.*

45 A. Bencini, G. Rajaraman, F. Totti and M. Tusa, *Superlattice Microst.*, 2009, **46**, 4.

46 K. Stokbro, J. Taylor, M. Brandbyge, J.-L. Mozos and P. Ordejón, *Comput. Mater. Sci.*, 2003, **27**, 151.

47 J. Huang, Q. X. Li, K. Xu, H. B. Su and J. L. Yang, *J. Phys. Chem. C*, 2010, **114**, 11946.

48 J. Huang, K. Xu, S. L. Lei, H. B. Su, Q. X. L. S. F. Yang and J. L. Yang, *J. Chem. Phys*, 2012, **136**, 064707.

49 Z. Q. Fan and K. Q. Chen, *Appl. Phys. Lett.*, 2010, **96**, 053509.

50 P. Zhao, Q. H. Wu, D. S. Liu and G. Chen, *J. Chem. Phys*, 2014, **140**, 044311.